


RESEARCH ARTICLE | MAY 13 2019

Surface coloring by laser irradiation of solid substrates

Huagang Liu ; Wenxiong Lin; Minghui Hong 



APL Photonics 4, 051101 (2019)

<https://doi.org/10.1063/1.5089778>



CrossMark




AMERICAN ELEMENTS
THE ADVANCED MATERIALS MANUFACTURER®

yttrium iron garnet glassy carbon beamsplitters fused quartz additive manufacturing
zeolites III-IV semiconductors gallium lump copper nanoparticles organometallics
nano ribbons barium fluoride europium phosphors photonics infrared dyes
sapphire windows Nd:YAG epitaxial crystal growth ultra high purity materials transparent ceramics CIGS
spintronics raman substrates cerium oxide polishing powder cermet nanodispersions
silver nanoparticles perovskites surface functionalized nanoparticles Al Si P S Cl Ar MBE grade materials thin film
MOCVD beta-barium borate K Ca Sc Ti V Cr Mn Fe Co Ni Cu Zn Ga Ge As Se Br Kr OLED lighting solar energy
rare earth metals quantum dots Rb Sr Y Zr Nb Mo Tc Ru Rh Pd Ag Cd In Sn Sb Te I Xe sputtering targets fiber optics
osmium scintillation Ce:YAG Cs Ba La Hf Ta W Re Os Ir Pt Au Hg Tl Pb Bi Po At Rn h-BN deposition slugs
refractory metals laser crystals Fr Ra Ac Rf Db Sg Bh Hs Mt Dst Rg Cn Nh Fl Mc Lv Ts Og CVD precursors photovoltaics

anodic aluminum oxide niobate InAs wafers Ce Pr Nd Pm Sm Eu Gd Tb Dy Ho Er Tm Yb Lu metamaterials borosilicate glass
MOFs AuNPs Th Pa U Np Pu Am Cm Bk Cf Es Fm Md No Lr YBCO superconductors InGaAs
ZnS CdTe perovskite crystals transparent ceramics indium tin oxide MgF₂ rutile optical glass

The Next Generation of Material Science Catalogs



Now Invent.™

www.americanelements.com

© 2001-2022, American Elements LLC, a U.S. Registered Trademark.

Surface coloring by laser irradiation of solid substrates

Cite as: APL Photon. 4, 051101 (2019); doi: 10.1063/1.5089778
Submitted: 22 January 2019 • Accepted: 19 April 2019 •
Published Online: 13 May 2019



View Online



Export Citation



CrossMark

Huagang Liu,¹  Wenxiong Lin,^{2,a)} and Minghui Hong^{1,a)} 

AFFILIATIONS

¹Department of Electrical and Computer Engineering, National University of Singapore, 4 Engineering Drive 3, 117576, Singapore

²National Engineering Research Center for Optoelectronic Crystalline Materials, Fujian Institute of Research on the Structure of Matter, Chinese Academy of Sciences, Fuzhou 350002, China

^{a)}Electronic addresses: elehmfh@nus.edu.sg and wmlin@fjirsm.ac.cn

ABSTRACT

Laser marking has become a versatile method for industrial product identification because of its applicability to almost all kinds of solid materials in a simple and single-step process. However, traditional laser marking generally produces contrast marks which are often monochromatic. There is increasing interest in color marking by laser processing for decoration and visual attraction. This tutorial provides a digest of the recent advancement of laser coloring technologies for surface coloration. An overview of existing methods for laser coloring is summarized, and three distinct physics mechanisms behind color formation are discussed. It is found that the coloration of diverse solid surfaces originates from laser induced oxidation, surface structuring, and micro/nanoparticles generation. How the laser processing parameters and experimental conditions affect the resulting colors is also presented. The laser coloring technique is capable of producing complete Hue palettes on metal surfaces by the precise control of laser processing parameters and will find much more extensive applications.

© 2019 Author(s). All article content, except where otherwise noted, is licensed under a Creative Commons Attribution (CC BY) license (<http://creativecommons.org/licenses/by/4.0/>). <https://doi.org/10.1063/1.5089778>

I. INTRODUCTION

As a versatile and environment-friendly technology, laser marking is rapidly replacing traditional marking methods such as painting and printing.¹ It has become a foremost industrial process today in many applications, such as the labeling of serial number, date, barcode, quick response (QR) code, company logo, trade marker, and other product information. Current laser marking typically produces monochromatic marks with gray or black color. However, there is greater interest in colorful marks or patterns for new applications, such as identification tags and product decoration.^{2,3} In addition, color marking is more appealing from an aesthetic point of view. Recently, color marking by laser processing without using any chemicals has emerged as a novel and versatile technology to create various colors on solid substrate surfaces. This laser color marking technology has received a great amount of research attention due to special advantages over traditional coloring methods (1) noncontact and operating without tooling requirement, (2) permanent wear resistant colors which do not fade over time, (3) high processing speed, high flexibility in automation, and low

operating cost (without using consumables), (4) ability to create precise features and various colors on a small area, (5) outstanding design flexibility in patterns and images because no molds or stencils are required, and (6) environmental friendliness due to the chemical free process.

Under the laser irradiation, physical or chemical effects usually occur on the substrate surface. The effects lead to the modification of optical properties in the visible range; as a result, various colors are created on the surface. Generally, laser color marking is mainly achieved through three approaches: thin film interference effect of the surface oxide layer,^{4,5} laser induced periodic surface structures (LIPSSs),^{6,7} and plasmonic colors excited from metallic nanoparticles and nanostructures.⁸ In the first approach, laser heating leads to the formation of a transparent or semitransparent oxide film on the substrate surface. With white light illumination, it can be reflected from the top and bottom surfaces of the oxide film. Constructive interference of the reflected beams makes the surface appear a certain color, which is determined by film thickness, refractive index of the oxide, and the order of interference. Some studies found that the intrinsic colors of the metal oxides play a more important role

in the surface color formation.⁹ The second approach of the laser coloring is to produce LIPSSs on substrate surfaces by high-peak-power femtosecond or picosecond lasers. The LIPSS acts as a grating to give rise to iridescent colors due to the optical diffraction effect. The colors are not caused by pigments but originate from material surface micro/nanostructures, namely, structural colors. The main feature of these structural colors is that they are highly dependent on a viewing angle. The third laser colorizing approach is also derived from the structural colors. Different from the second mechanism, the surface structures which excite the surface colors are randomly distributed without regularity, and the color does not vary with the viewing angle. Surface plasmon resonance (SPR) effects arising from metallic nanostructures and nanoparticles are the main causes for this type of coloring.

The scope of this tutorial is to present the recent advancement and the fundamental basics of laser color marking for surface coloration and decoration. An overview of the existing methods for laser color marking is provided, and several possible mechanisms responsible for the surface color formation are discussed. How the laser processing parameters and experimental conditions affect the resulting colors is also presented. Some important applications of the laser color marking are also introduced.

II. EXPERIMENTAL

For the laser color marking, relative motion between the laser beam and sample is required. There are two commonly used methods to achieve the relative motion. The first one is to scan the beam over the sample by using two galvanometer-driven scanning mirrors, while the second method is to move the sample under a fixed beam by computer-controlled 2D or 3D translation stages. The experimental setups for the laser color marking are shown in Fig. 1.

The laser coloring can be achieved by nanosecond, picosecond, and femtosecond laser irradiation, with the wavelength ranging from UV to IR. The laser parameters which have significant impacts on the colors being produced are power, wavelength, pulse width, repetition rate, and beam size. Usually, each color is associated with a set of laser parameters. The key of the laser processing is to find the correspondence between the color and parameter set. In addition to the laser parameters, there are some other factors which also affect the produced colors: processing parameters, ambient condition,

and sample properties. Processing parameters include scanning speed, line spacing, defocusing value, and number of scanning. Ambient conditions refer to surrounding temperature and atmosphere. Most of the laser coloring experiments are performed at room temperature and atmospheric environment. The influences of different ambiances, such as oxygen, nitrogen, inert gas, and liquid on the surface coloring, have also been studied. Sample properties mainly refer to the compositions of the substrate, surface roughness, and substrate thickness, which significantly affect the compositions of the formed oxides and the types of the surface structures. Most studies of the laser coloring focus on metal and alloy substrates as they are easy to be oxidized and structured in air. Some metal oxide and semiconductor materials can also be color marked by laser irradiation. Table I provides a summary of the laser coloring research on different substrates, for different lasers and key parameters used.

III. LASER COLORING FROM SURFACE OXIDATION

Laser induced oxidation is a well-known phenomenon because substrate materials react much easily with oxygen under the assist of laser heating. As early as the 1980s, laser induced oxidation has been extensively studied on a variety of materials, such as silicon (Si), chromium (Cr), cadmium (Cd), copper (Cu), and tellurium (Te).^{27–30} It was found that the oxide films produced on Cd, Cu, and titanium (Ti) surfaces exhibit colors which are different from the substrates.^{28,31} Thus, laser processing provides a possibility to create permanent colors on sample surfaces by controlling the oxide layer formation. This color marking technique was extensively studied on numerous metals and alloys with a variety of lasers. Being a most widely used alloy, stainless steel is the most studied material. Laser colorizing has been demonstrated on various grades of stainless steels, such as 304,^{10,32} 304L,^{33,34} 316,¹³ 316L,³⁵ and even a home-made stainless steel with definite compositions.¹³ Since the produced colors are governed by laser induced oxide films, the control of the oxide film thickness and composition is essential to the surface performances.^{11,12,33,34} Systematic studies of the oxide layer formation and the influences of various laser processing parameters on the produced colors have been studied.^{5,36} Through the precise adjustment of the laser parameters and process parameters, a variety of colors and even complete color palette³⁷ can be obtained. Figure 2 shows a matrix palette produced on a 304 grade stainless steel surface

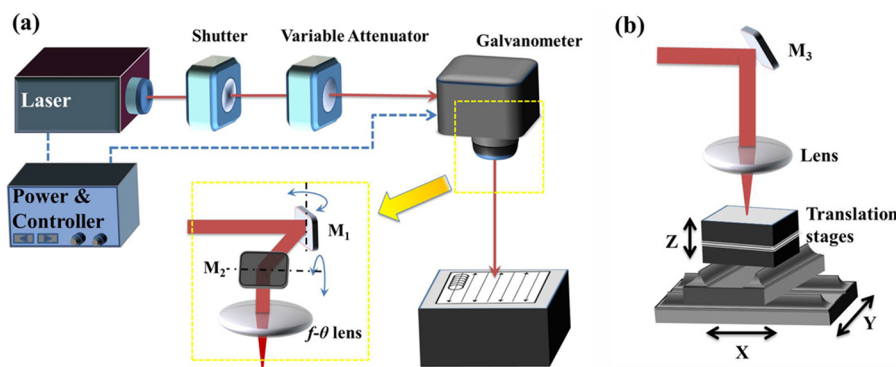


FIG. 1. Experimental setups for laser color marking: (a) galvanometer scanning and (b) translation stages. M_1 , M_2 , and M_3 are mirrors.

TABLE I. A summary of the laser color marking on different substrates by different lasers. λ : wavelength; τ : pulse width; f : repetition rate; v : scanning speed; l : line spacing; and SS: stainless steel.

Mechanisms	Substrates	Lasers	Parameters: λ ; τ ; f ; v ; l
Surface oxidation	SS 304	Yb:glass fiber laser ¹⁰	1062 nm; 100 ns; 20–100 kHz; 50–225 mm/s; 10–50 μ m
		3rd-harmonic Nd:YVO ₄ laser ¹¹	355 nm; 25 ns; 40 kHz; 400–500 mm/s; 30 μ m
		Yb pulsed fiber laser ¹²	1060 nm; 100 ns; 20–99 kHz; 1–250 mm/s; -
	SS 316	Yb pulsed fiber laser ¹³	1064 nm; 100 ns; 20–100 kHz; 10–500 mm/s; -
		KrF excimer laser ⁵	248 nm; 20 ns; 225 kHz; -; -
	SS SU303	Nd:YAG laser ¹⁴	1064 nm; 300 ns; 30 kHz; 25–300 mm/s; 200 μ m
		Pulsed fiber laser ¹⁵	1064 nm; 119 ns; 225 kHz; 90–600 mm/s; 10 μ m
	Pure Ti	Yb pulsed fiber laser ¹²	1060 nm; 100 ns; 20–99 kHz; 1–250 mm/s; -
		Fiber ns laser ¹⁶	1064 nm; 15–225 ns; 500 kHz, 1 MHz; up to 2500 mm/s; -
		Nd:YAG ns laser ³	1064 nm; 100 ns; 20 Hz; 3–100 mm/s; -
Ti-6Al-4V	WO ₃	KrF excimer pulse laser ¹⁷	248 nm; 23 ns; 10 Hz; -; -
LIPSS	SS	Ti:sapphire fs laser ¹⁸	800 nm; 90 fs; 1 kHz; 1–4 mm/s; 50 μ m
		Ti:sapphire fs laser ⁷	800 nm; 150 fs; 5 kHz; 10–130 mm/s; -
		Ti:sapphire fs amplifier- OPA ¹⁹	240 nm–2600 nm; 1 kHz; 13 mm/s; -
	Cu	ps laser ²⁰	1064 nm; 10 ps; 203.6 kHz; -; -
		Ti:sapphire fs laser ²¹	800 nm; 65 fs; 1 kHz; -; -
	Ag	Ti:sapphire fs laser ²²	800 nm; 120 fs; 1 kHz; 0.1–16 mm/s; 50 μ m
		Ti:sapphire fs laser ⁶	800 nm; 65 fs; 83 Hz; 1 mm/s; -
	Al	Ti:sapphire fs laser ²³	744 nm; 100 fs; 10 Hz; 0.02–0.6 mm/s; -
		Ti:sapphire fs laser ²⁴	800 nm; 65 fs; 1 kHz; 1 mm/s; -
	Ti	Ti:sapphire fs laser ²⁵	800 nm; 100 fs; 1 kHz; 1 mm/s; -
Si		Ti:sapphire fs laser ²⁵	800 nm; 100 fs; 1 kHz; 1 mm/s; -
Nanoparticles and nanostructures	Ag	Nd:YVO ₄ ps laser ⁸	1064 nm; 10 ps; 50 kHz; 11–3000 mm/s; 1–13.5 μ m
	Cu	Nd:YVO ₄ ps laser ²⁶	1064 nm; 10 ps; 100 kHz, 200 kHz, 1 MHz; 50–5000 mm/s; 10–20 μ m
	Al	Ti:sapphire fs laser ⁶	800 nm; 65 fs; 100 Hz; 1 mm/s
	Au	Nd:YVO ₄ ps laser ⁸	1064 nm; 10 ps; 50 kHz; 11–3000 mm/s; 1–13.5 μ m

by a nanosecond fiber laser in raster scanning. Rich colors are produced at different scanning speeds and line spacings. The laser coloring technique shows wide potential applications in colorful tags and logos, decorative artwork, and product identification. Some

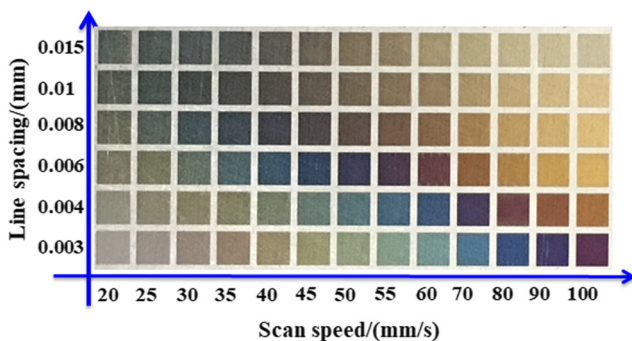


FIG. 2. A matrix palette produced on 304 grade stainless steel at different powers and line spacings. Repetition rate: 300 kHz; laser power: 4.5 W; and pulse width: 10 ns.

applications of laser coloring are presented in Fig. 3, where color bar code, World Cup logo, and some artwork images are marked on stainless steel surfaces, demonstrating the ability of laser coloring to create exquisite images and patterns on metal substrates.

Many studies of the laser color marking have been focused on Ti and its alloys because of their wide range of applications. Carey *et al.* demonstrated the laser coloring of Ti jewelry with a pulsed Nd:YAG laser,² establishing the viability of laser coloring in the ornamentation of craft metal work and jewelry. By controlling the oxide growth, O'Hana *et al.* used the laser as a “pen” to produce precisely defined colors for fashion metal jewelry design and decoration.³ Further studies on pure Ti and its alloys have been performed to reveal the physics mechanisms behind the laser color marking,^{4,12} to analyze compositions and structures of the oxide film,^{4,38–41} and to investigate the effects of laser processing parameters on the resulting colors.^{2,14–16} Similar to stainless steel, a wide spectrum of colors has been achieved on Ti and its alloys. Figure 4 shows a series of colors produced on Ti substrates at different scan speeds and different laser powers.¹⁵ Figure 5 shows a International Commission on Illumination (CIE) 1931 x-y chromaticity diagram of laser-induced Ti oxide layers.¹⁵ It can be seen that the obtained colors span a large range of x and y values, which are vibrant but not saturated. However,

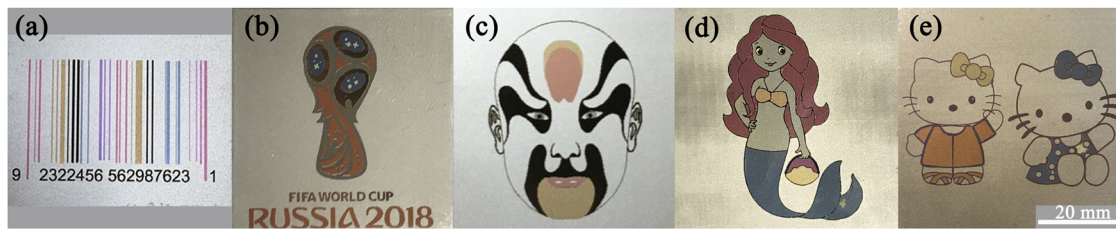


FIG. 3. Demonstration of applications of laser coloring on stainless steel. (a) Color bar code, (b) FIFA World Cup logo, (c) facial markup, and [(d) and (e)] cartoon images.

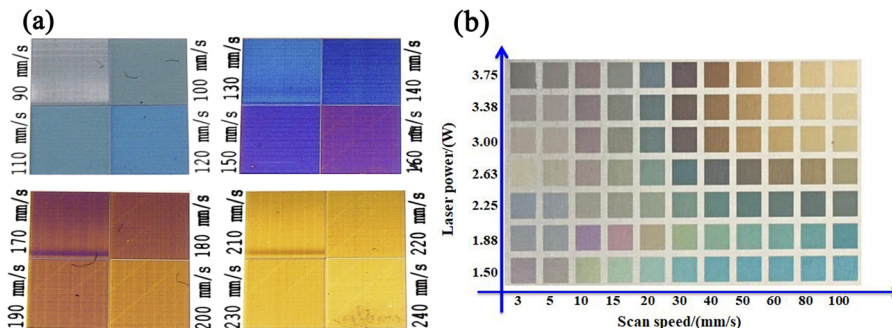


FIG. 4. A variety of colors produced on Ti substrates by varying laser parameters. (a) Colors produced at different scan speeds and a fixed laser power.¹⁵ Reproduced with permission from Adams *et al.*, Surf. Coat. Technol. **248**, 38–45 (2014). Copyright 2014 Elsevier B. V. (b) Color matrix by varying scan speed and laser power.

the obtained colors do not cover the integral visible range. Red and green colors cannot be achieved on Ti surfaces by the laser oxidation method. This phenomenon may be attributed to the film thickness, which becomes too big for the origin of interference effects inside the film.¹²

In addition to metals and alloys, some oxide substrates can also be colored by lasers. Lu and Qiu reported that the surface color of an amorphous WO_3 thin film could be modified from brown to purple by a 248 nm KrF excimer laser, and the color could be thermally bleached back to brown by a Nd:YAG laser.¹⁷

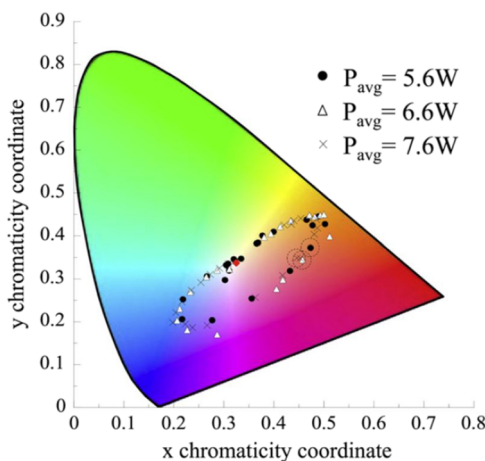


FIG. 5. Chromaticity of various titanium oxide coatings produced at laser powers of 5.6, 6.6, and 7.6 W plotted over the CIE 1931 color space.¹⁵ The red diamond symbol is the measured x and y chromaticity of a bare Ti substrate. Reproduced with permission from Adams *et al.*, Surf. Coat. Technol. **248**, 38–45 (2014). Copyright 2014 Elsevier B. V.

Physical mechanisms underlying the laser coloring by the surface oxidation have been discussed in a number of the previous studies.^{4,14,33,40} Laser oxidation of metals is a process of fast gaseous corrosion occurring at high temperatures. The laser oxidation process and oxide layer growth are roughly divided into 5 stages:¹³ (1) heating of the metal surface by laser radiation. Upon metals being exposed to laser irradiation in air or oxygen environments, the laser energy is provided to electrons which are then excited from the lower energy state to the higher energy state. Then, the excited electrons decay rapidly to their fundamental state by releasing their energy to the lattice and produce a temperature increase to the irradiated area. (2) Reaction between the oxygen of air and the metal occurs due to high temperatures. The oxidation process starts from a physical adsorption of oxygen on the metal surface. (3) The 2nd stage is followed by the dissociation of the oxygen-oxygen liaisons and formation of ionic liaisons between oxygen free electrons and the metallic ions. Then, the first oxide germ is formed on the surface. (4) The oxide germ grows laterally, leading to the formation of a continuous thin metal oxide film on the laser irradiated area. (5) The cation/anion diffusion at the interface of the metal/oxide results in a perpendicular growth of the oxide. In theory, based on the thermodynamic data and kinetic coefficients, the reaction course and products of the laser oxidation may be foreseen. However in real conditions, the laser heating process introduces a series of complex factors, which leads to the oxidation to be a nonisothermal process. The process is nonlinear and takes place in nonequilibrium circumstances. In the case of short laser pulse, the temperature variation may be faster than the chemical reactions. In addition, the reaction rate is high due to local high temperatures. Therefore, the laser oxidation process is complicated, and the oxidation kinetics is different from the isothermal process. It is hard to give a universal physical-chemical mechanism to describe the process.⁴² On the other hand, it is possible to obtain the regulation of the laser oxidation process for

a given metal via experimental studies. The connection between the oxide layer and the laser parameters can be found through the quantitative analyses of the oxide layer characteristics (chemical compositions, thickness, and crystallinity). An example of the investigation on the oxidation process is demonstrated in Ref. 14. It is found that as the laser fluence increases from 54 to 648 J/cm², the characteristic signals of Ti₂O, TiO, TiO₂, and Ti₂O₃ appear successively from XRD diffractograms. The onset of each different oxide occurs at a specific accumulated laser fluence, and the higher the laser fluence, the higher the degree of oxidation. The studies on the laser oxidation of stainless steel also show that the proportion of oxides (Cr₂O₃, Fe₂O₃, MnO, and NiO) varies with different laser processing parameters,⁹ suggesting that the oxidation kinetic process has a strong dependence on the laser parameters.

Two main mechanisms have been suggested to explain how the oxide layers exhibit different colors. The first one is based on the thin film effect. As illustrated in Fig. 6, a white illumination light can be reflected from the surfaces of both the oxide film and the metal. The optical path difference δ between the two reflected beams can be expressed by the following formula:

$$\delta = \frac{2h}{\sqrt{n_1^2 - \sin^2 \theta_i}}, \quad (1)$$

where h , n_1 , and θ_i are the oxide film thickness, refractive index of the oxide film, and the incidence angle, respectively. When the optical path difference $\delta = k\lambda$ (k is an integer) for a wavelength λ , the specific color is enhanced due to the constructive interference. Equation (1) indicates that the enhanced color is dependent on the thickness and refractive index of the oxide layer, viewing angle, and order of interference. This laser color marking mechanism is confirmed by the experimental observation of the oxide film interference and the surface color changing with viewing angle. Strong oscillations of reflected light intensity were measured on a laser-induced oxidation surface of Cu.³⁰ Variation of observed colors with the oxide thickness has also been demonstrated on laser color marked Ti substrates.^{4,15} XRD spectra of laser treated Ti samples revealed that the oxide film is a mixture of several Ti oxides, as shown in Figs. 7(b) and 7(c).⁴ Detailed microstructures and phase analyses show that the oxide film is composed of a thin layer of TiO₂ rutile formed at the surface and a mixture of Ti oxides with a lower degree of oxidation (TiO and other oxides) below the TiO₂ layer. The oxide thickness increases with laser fluence, giving rise to different observed colors due to the interference between the reflected light from both surfaces of the TiO₂ layer. This interference effect was also confirmed by experiments on stainless steel,⁵ where the laser-induced colors were

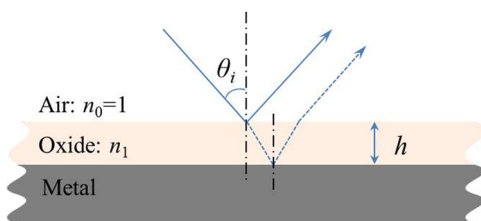


FIG. 6. Schematic diagram of the interference effect of the oxide film. n_0 and n_1 are the refraction indices of air and oxide, respectively.

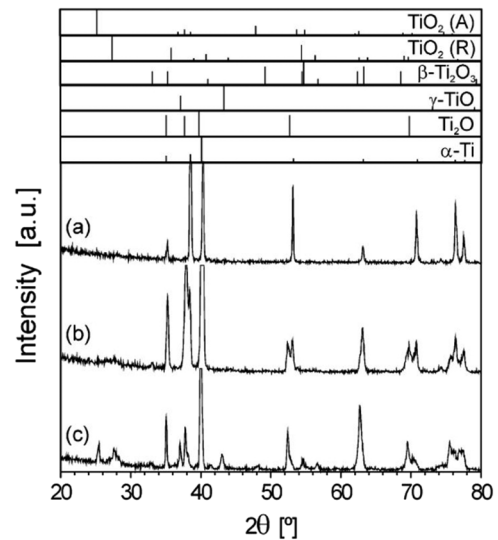


FIG. 7. Grazing incidence X-ray diffractometry spectra of (a) an anodized sample for comparison and laser treated samples obtained at the scanning speeds of (b) 240 and (c) 80 mm/s.⁴ In addition, the powder diffraction patterns corresponding to α -Ti, Ti₂O, γ -TiO, β -Ti₂O₃, and TiO₂ rutile (R) and anatase (A) are also presented. Reproduced with permission from Del Pino *et al.*, *Surf. Coat. Technol.* **187**(1), 106–112 (2004). Copyright 2004 Elsevier B. V.

found to vary with the oxide thickness. The reflectance spectrum of the laser marked surface as a function of incidence angle of the probe light (i.e., viewing angle) has been measured.³⁷ It is shown that not only the color brightness and saturation but also the color hue vary with viewing angle. The reflectance spectrum is blue-shifted as the angle increases.

The second mechanism of the laser coloration effect is attributed to the intrinsic colors of the metal oxides. Compositional analyses and structural studies of the laser induced Ti oxide films have been performed,^{14,31,38} where there is a certain correlation between the final surface colors and compositions of the laser-induced oxide films. For example, golden color is the same as bulk TiO;¹⁴ the purple is the color of Ti₂O₃, which is confirmed by XRD analyses;³¹ and the white layer may attribute to the presence of TiO₂ anatase.³¹ Lu *et al.* studied the laser coloration mechanism of 304 grade stainless steel through the quantification analyses of surface compositions.⁹ The colors of laser marking are dominantly contributed to the colorful oxides and spinel compounds, which act as natural pigments presenting distinct colors.

The two physics mechanisms on the laser induced colors are both reasonable and supported by numerous pieces of experimental and theoretical evidence. A systematic study of Ti and stainless steel substrates suggests that both the interference effect and the intrinsic color of oxide films contribute to the final surface colors.¹² Which one is dominant depends on the specific color and substrate properties.

For practical applications, the key factor is to control the formation of the oxide film accurately so that to obtain desired colors. Regardless of which mechanism is, the oxide layer thickness and composition are the dominant factors in determining the final

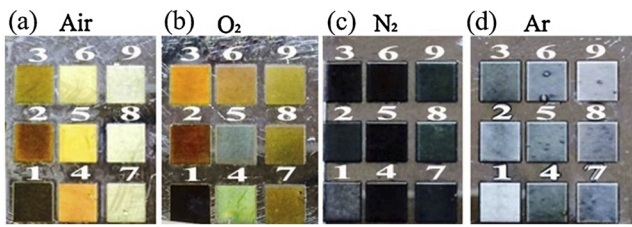


FIG. 8. Photographs of the stainless steel surfaces processed by a nanosecond laser in various gases.⁴⁵ Samples 1–9: the laser scanning speed was varied from 10, 20, 30, 40, 50, 60, 70, 80 to 90 mm/s. Reproduced with permission from Luo *et al.*, *Appl. Surf. Sci.* **328**, 405–409 (2015). Copyright 2015 Elsevier B. V.

surface colors, which are eventually determined by several factors, including laser processing parameters, ambient condition, and sample properties. How these parameters or conditions affect the oxide films and the resulting colors has been studied. Li *et al.* studied the processing of UV laser-induced surface coloration and photothermal oxidation of stainless steel.¹¹ The results show that the colors produced by laser irradiation are affected by processing parameters, including laser power, focal plane offset, scanning direction and speed, and repetition scanning number. A systematic research on the relation of laser parameters to the obtained colors was performed by using a master oscillator power amplifier (MOPA) fiber laser,³⁶ where pulse energy and its peak power are considered as the main limiting factors to produce high quality surface colors. The required colors can be obtained by selecting correct pulse energy and proper peak power by optimizing the pulse width. Lavisse *et al.* demonstrated that laser fluence has a significant influence on the colors obtained.⁴³ When the laser fluence was varied from 4 to 60 J/cm², the surface color changed from colorless and yellow for low fluence (<25 J/cm²) to purple and blue at a higher fluence. Antończak *et al.*

studied the sensitivity scaling of a number of laser processing parameters on laser color marking of stainless steel.¹⁰ The impact of each laser processing parameter was analyzed separately. This study offers an accessible approach to achieve greater stability and repeatability for industrial applications of the laser color marking.

Since the laser induced colors are attributed to the oxide film formed by the reaction of the substrate material with surrounding oxygen, the ambient environment must have major influences on the produced colors. Zheng *et al.* reported experimental results of laser marking in different gas ambiances, such as O₂, N₂, Ar, and He.^{5,44} High O₂ concentration can help to speed up the oxidation and reduce the number of required laser pulses. On the other hand, in a low O₂ ambience, the oxidation process is slowed down, however, enabling a finer control of the growth of the oxide layer and the surface colors.⁴⁴ Luo *et al.* also found that the O₂ concentration can greatly affect the surface morphology and chemical compositions of the produced oxide films and therefore affect the surface colors.⁴⁵ Laser processing was performed in four different gaseous environments: air, O₂, N₂, and Ar. All photographs of the laser processed surfaces are shown in Fig. 8. It can be seen that colorful surfaces were obtained in O₂ and air environments, and the surface created in O₂ presents much richer colors than those in air. On the other hand, however, in the oxygen-free environment (N₂ and Ar environments), only dark and gray surfaces were obtained. This is because that more oxides are produced at oxygen-rich conditions, which exhibit more colors due to film effects or their instinct colors. In addition, environmental temperature is also an important factor affecting the laser induced colors.¹⁰

The final colors of laser treated surfaces are also highly dependent on substrate composition and thickness. Although with the same laser processing parameters, different colors can be obtained on several stainless steels by varying chemical compositions.¹³ Because the laser coloring process is driven by laser heating, the substrate thickness can have significant impact on the resulting colors.

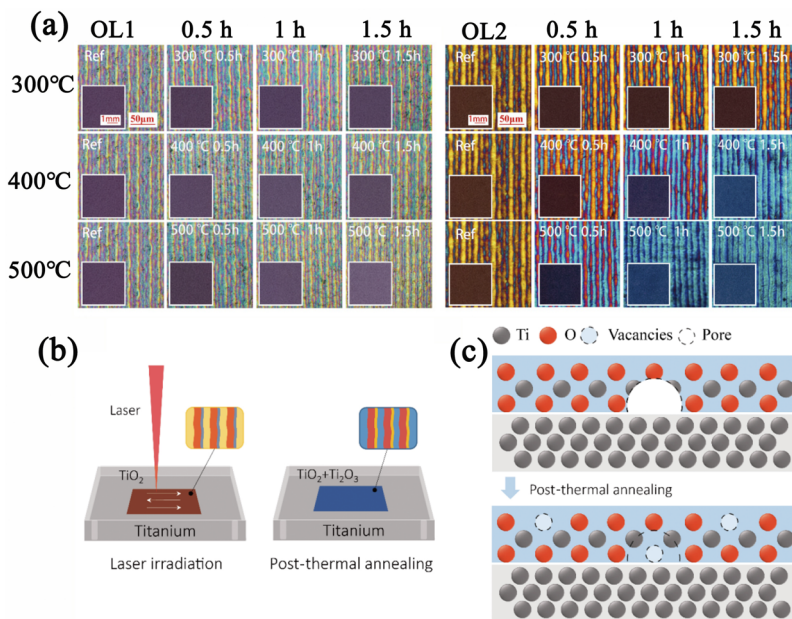


FIG. 9. (a) Microscope images and surface colors (insets) of two sets of samples [oxide layer 1 (OL1) and oxide layer 2 (OL2)] before and after the thermal annealing at 300, 400, and 500 °C, duration of 0.5, 1.0, and 1.5 h, respectively. (b) The color tuning process via the post-thermal annealing. (c) The model of the oxidation process during the annealing.⁴⁶ Reproduced with permission from Zhou *et al.*, *Appl. Sci.* **8**(10), 1716 (2018). Copyright 2018 MDPI Journals.

A thick substrate can provide a bulk heat-sinking capability. On the contrary, thin substrate may suffer from serious thermal effects.³⁵ The difference of substrate temperature leads to different surface colors.

Finally, it is noted that surface colors produced by the laser marking can also be tuned by post-treatment.⁴⁶ Thermal annealing has been performed on laser colored Ti substrates. Two sets of samples before and after the thermal annealing are shown in Fig. 9(a). It is found that the post-treatment can increase the color lightness and lead to a color hue change. The color shift depends on annealing temperature and duration. Composition analyses of the surface oxide film reveal that thermal annealing leads to further oxidation and generates a new oxide, which changes the surface color. The schematic diagrams of color tuning and oxidation process during the annealing are illustrated in Figs. 9(b) and 9(c).

IV. ANGLE DEPENDENT COLORS ARISING FROM LIPSSs

There is a category of colors called structural colors,⁴⁷ which are not caused by pigments or dyes but intrinsically generated from light diffraction, interference, or scattering from micro/nanostructures. One approach to obtain structural colors is to utilize laser-induced LIPSSs. LIPSSs are regular groove structures with a spatial period on the wavelength scale produced by laser irradiation. Like a one-dimensional grating, the LIPSSs can give rise to structural colors due to the diffraction effect. LIPSSs were first observed by Birnbaum on semiconductor materials using a ruby laser.⁴⁸ They were then extensively studied on various semiconductors,^{49,50} metals,^{7,51} and dielectrics.^{50,52}

The generation of LIPSSs provides a simple way to control the surface optical properties and visual colors of metals. Various colors have been observed on a variety of metals, such as Al,^{6,22} Ag,²¹ stainless steel,^{7,18,19} and Cu.²⁰ The LIPSS-generated colors are highly dependent on viewing angle. Figure 10 shows an Al sample produced by femtosecond laser processing, which exhibits various colors at different viewing angles.⁶ SEM images reveal that LIPSSs are produced on the laser irradiated region, which caused the angle-dependent colors, as shown in Fig. 10(b). The LIPSS period is about 540 nm and much less than the laser wavelength of 800 nm. The LIPSSs are significantly polarization dependent with the periodic structure orientation perpendicular to the incident laser polarization for metal substrates. This characteristic makes it possible to control the surface visual colors through controlling the laser beam polarization. Colorful pictures and patterns on metallic surfaces have been demonstrated by producing a set of LIPSSs along different orientations.^{7,18}

Structural colors of the LIPSSs have also been observed on semiconductors.^{24,25,53} Vorobyev and Guo studied the formation and the effects of femtosecond laser induced LIPSSs on a silicon wafer.²⁴ A unique nanostructured grating at a period of 575 nm was produced, and the laser structured area exhibits various colors at different viewing angles, which is similar to the angle effects of metal LIPSSs. However, the structural colors are much darker than those on metals. Yang *et al.* performed a comparative study on laser coloring of silicon based LIPSSs in different ambiances, such as air, vacuum, and nitrogen.⁵³ It is found that LIPSS-generated structural

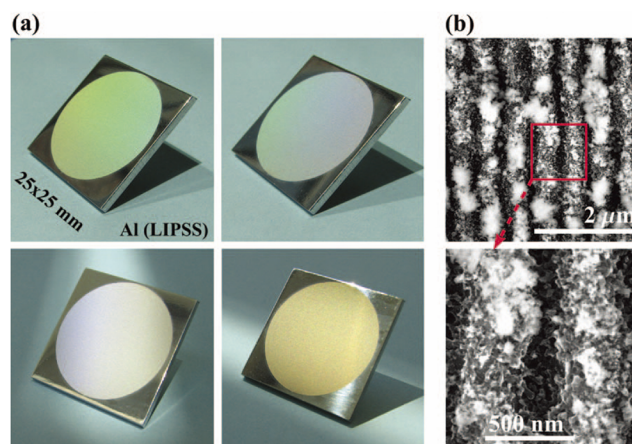


FIG. 10. An angle-dependent color Al samples produced by laser-induced LIPSSs.⁶ (a) Photographs show that the surface color varies with viewing angle. (b) SEM images showing the LIPSSs on the color Al sample. Reproduced with permission from A. Y. Vorobyev and C. Guo, *Appl. Phys. Lett.* **92**(4), 041914 (2008). Copyright 2008 AIP Publishing LLC.

colors in a vacuum and nitrogen are clearer than those produced in air, as presented in Fig. 11. Low-oxygen ambience can improve the brightness of structural colors. A further study of femtosecond laser processing of silicon has observed that long and deep grooves lead to the redistribution of the incident laser light inside the grooves.²⁵ As a result, one- and two-dimensional nanohole arrays can be produced on the laser irradiated area. Such a surface decorated with high-density nanoholes exhibits vivid structural colors covering the entire visible spectrum.

LIPSS is a self-organized laser structuring. Generally, the LIPSSs have a period close to the laser wavelength and orient perpendicular to the polarization of the incident laser beam for metal and

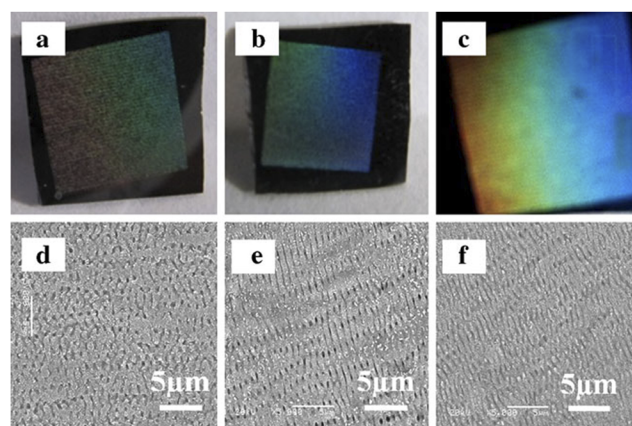


FIG. 11. Photographs of colored silicon in (a) air, (b) vacuum, and (c) N₂.⁵³ The corresponding SEM images in (d) air, (e) vacuum, and (f) N₂. Reproduced with permission from Yang *et al.*, *Appl. Phys. A* **104**(2), 749–753 (2011). Copyright 2011 Springer-Verlag.

semiconductor substrates. Formation of the surface ripples implies that there should be a mechanism allowing for the incident laser light to couple with the surface and create ripples on it. According to the classical theory, surface scattering waves are considered as one of the possible sources as they are able to provide the required coupling with the incident laser light. For an ideally flat surface, the incident light is reflected with $\theta_i = \theta_r$, and there is no light coupling on the surface. For a surface with random roughness, interference between the incident light and the surface scattered wave occurs, when the wave vector of a harmonic Fourier component of the surface roughness \mathbf{g} satisfies⁵⁴

$$\mathbf{K}_{ip} \pm m\mathbf{g} = \mathbf{K}_{sp} \quad (m = 1, 2, 3 \dots) \quad (2)$$

Equation (2) is also called momentum conservation law, where \mathbf{K}_{ip} and \mathbf{K}_{sp} are the wave-vector component parallel to the surface of the incident light and the wave vector of the surface wave. The geometry relationship of these wave vectors on a substrate surface is presented in Fig. 12. When $m = 0$, the period of the interference pattern $\Lambda = 2\pi/|\mathbf{g}|$, i.e., the period of the LIPSS can be derived^{54,55}

$$\Lambda = \frac{\lambda}{n \pm \sin \theta_i}, \quad (3)$$

where λ , θ_i , and n are laser wavelength, incidence angle, and refractive index of material, respectively. This explanation agreed well with the experimental observation using continue wave (CW), nanosecond even picosecond pulsed lasers.⁵⁶ With the advancement of femtosecond pulsed laser technologies, more complex LIPSSs were observed on different materials, challenging the established classical model.⁵⁷ Some LIPSSs produced under the irradiation of the femtosecond laser are characterized by much smaller periods than laser wavelength or by a high dependence on laser fluence,^{50,58} which cannot be explained by Eq. (3). The surface plasmon polaritons (SPPs) were introduced to explain the femtosecond laser induced LIPSSs.^{58,59} It is well known that the incident light can couple to SPPs via nanoroughness on the metal surface due to diffraction.⁶⁰ The interference between the incident light and the excited surface plasmon waves leads to a periodic spatial modulation of the surface energy distribution and results in the formation of periodic structures. The period Λ is given as follows:^{59,61}

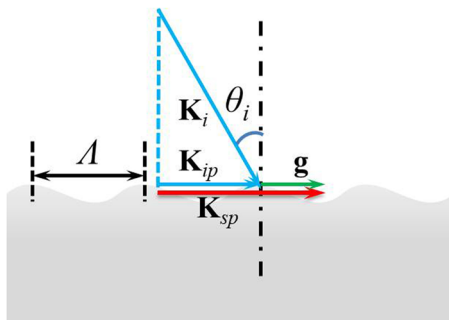


FIG. 12. The geometry of light incident on a substrate surface. \mathbf{K}_{ip} is the wave-vector component parallel to the surface of the incident light, \mathbf{K}_{sp} is the wave vector of the surface wave, \mathbf{g} and Λ are the wave vector and period of the surface period structures, respectively, and θ_i is the incident angle.

$$\Lambda = \frac{\lambda}{\text{Re}[\eta] \pm \sin \theta_i}, \quad (4)$$

where $\eta = [\epsilon_d \epsilon_{metal} / (\epsilon_d + \epsilon_{metal})]^{1/2}$ is the effective refractive index of the surface plasmons at the dielectric-metal interface and ϵ_d and ϵ_{metal} are the dielectric constants of the ambient medium and the metal, respectively. Moreover, there is another type of LIPSS (often referred to as high-spatial-frequency LIPSS) that has a period much smaller than laser wavelength.^{62,63} The formation of the high-spatial-frequency LIPSSs can be explained by the polariton model.⁶⁴ The interference between the incident laser and the spatial harmonics of the excited SPPs results in a finer periodic modulation on the samples surface, leading to the formation of periodic nanostructures with the period equal to or even as a fraction of the incident wavelength ($\lambda/2^m$, $m = 0, 1, 2, \dots$). In addition, other mechanisms have also been introduced to explain the formation of high-spatial-frequency LIPSSs, such as self-organization

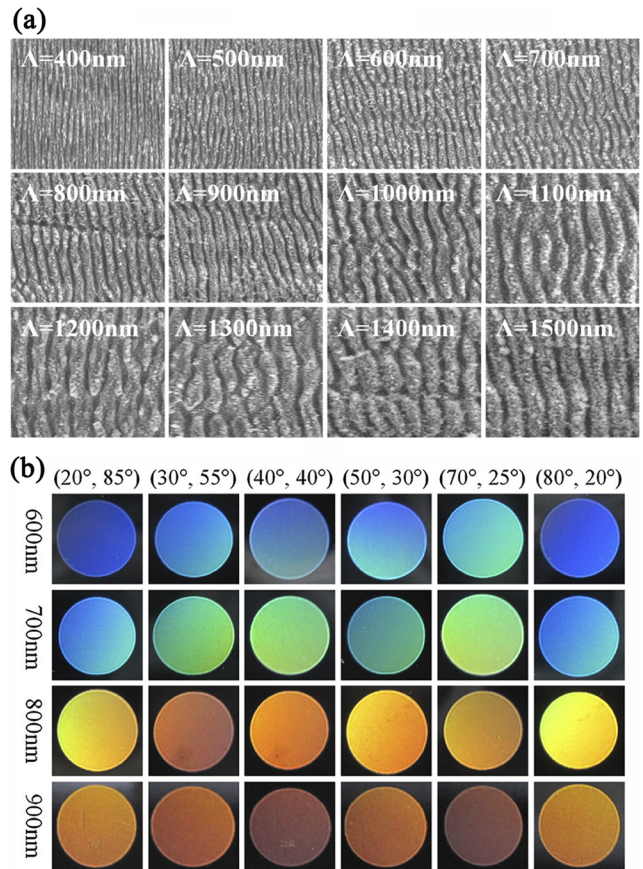


FIG. 13. (a) LIPSSs of different spatial periods produced with different laser wavelengths.¹⁹ (b) Various iridescent colors on stainless samples with different periods. The vertical axis represents the LIPSS period. The first number in the bracket is the angle between the illumination and the normal direction (Z), and the second number is the angle between the ripple and the horizontal direction (X). Reproduced with permission from Li *et al.*, Appl. Phys. A 118(4), 1189–1196 (2015). Copyright 2015 Springer-Verlag.

from laser-induced surface instability⁶⁵ and second-harmonic generation.⁴⁹

The physical processes and the evolution of femtosecond laser induced LIPSS formation are investigated on the Ti material.⁶⁶ At the first few laser pulses, randomly distributed nanostructures are produced on the surface. Then, the next laser pulses excite SPPs on the substrate surface, which couple with the incident laser via the previously produced nanostructures.⁶⁰ The coupling effect causes the periodic spatial modulation of the energy deposited on the irradiated area and leads to the formation of nascent periodic structures. As the laser spots continue to increase, the nascent periodic structures grow and become more regular.

Equation (4) gives the dependence of LIPSS period on laser wavelength, incidence angle, and real part of the effective refractive index. Controllable formation of LIPSSs at different periods has been demonstrated by varying laser wavelength,^{19,67} incidence angle,⁶⁸ ambient dielectric medium,^{69,70} and laser fluence.^{50,58} An example of laser color marking at different wavelengths is demonstrated in Ref. 19, as illustrated in Fig. 13, where the LIPSSs with periods from 400 to 1500 nm were produced on stainless steels using a wavelength-tunable femtosecond optical parametric amplifier. The LIPSSs at different periods exhibit various iridescent colors with different viewing angles. The effect of the laser incidence angle on the LIPSS period has been studied in Ref. 23. Bright colors covering the entire visible range were achieved via predetermined variation of the laser incidence angle and the change of ripples period.

V. ANGLE-INDEPENDENT COLORS ARISING FROM MICRO/NANOSTRUCTURES

As discussed above, structural colors arising from LIPSSs are angle dependent. However, some research studies on laser color marking using femtosecond or picosecond lasers have shown that the treated surfaces exhibit fixed colors which do not vary with viewing angle. Localized SPR effects arising from metallic nanostructures and nanoparticles have been suggested to explain the angle-independent color production. In order to simplify the physical model, a spherical nanoparticle of a radius a is considered. When the nanoparticle is irradiated by a z -polarized light at a wavelength λ , which is much larger than a , by solving Maxwell's equations using a quasistatic approximation, the electromagnetic field (E_{out}) outside the nanoparticle can be given⁷¹

$$E_{out}(x, y, z) = E_0 \hat{z} - \left[\frac{\epsilon_{in} - \epsilon_{out}}{\epsilon_{in} + 2\epsilon_{out}} \right] a^3 E_0 \left[\frac{\hat{z}}{r^3} - \frac{3z}{r^5} (x\hat{x} + y\hat{y} + z\hat{z}) \right], \quad (5)$$

where ϵ_{in} is the dielectric constant of the metal nanoparticle and ϵ_{out} is the dielectric constant of the external environment. The dielectric constant of the metal ϵ_{in} is dependent on the incident light wavelength. When ϵ_{in} is roughly equal to $-2\epsilon_{out}$, the electromagnetic field is significantly enhanced at the corresponding wavelength. This surface plasmon resonance leads to an absorption enhancement at the resonant wavelength.^{72,73} When the enhanced absorption wavelengths are in the visible range, the surface reflection properties

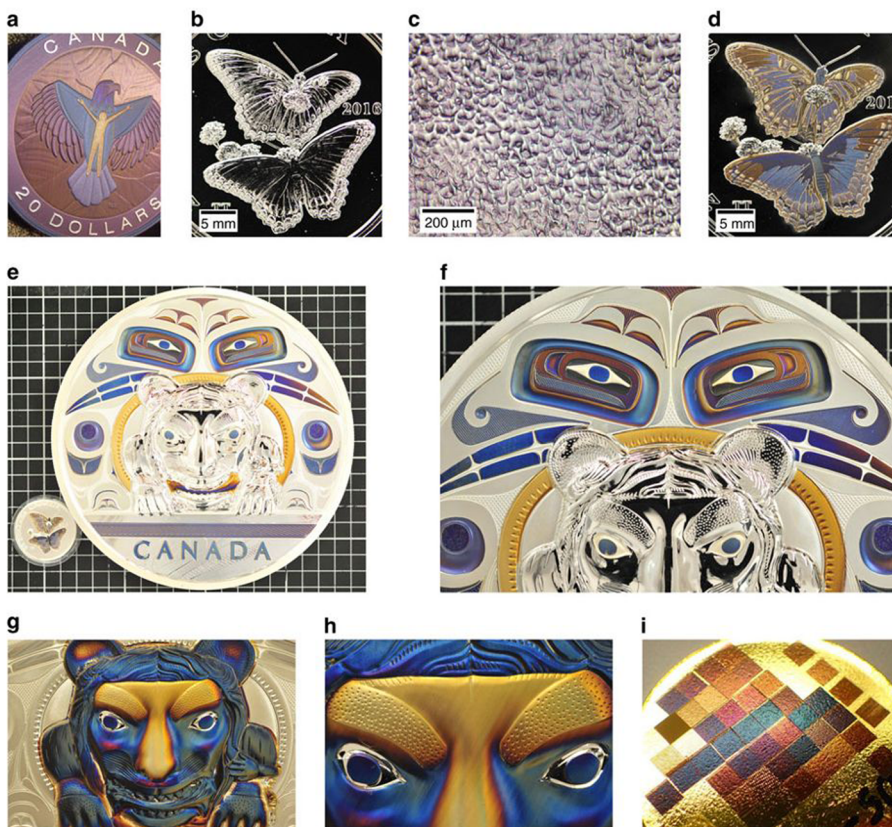


FIG. 14. Demonstration of noniridescent coloring of metal surfaces.⁸ (a) Photograph of a colored silver coin featuring a representation of an eagle. [(b) and (d)] Photographs of silver coins bearing a frosted butterfly (b) before and (d) after laser coloring. (c) Microscope image of the frosted regions, having topographic variations of up to 2 mm in height and a roughness of $\sim 1\text{--}2\ \mu\text{m}$. (e) Photograph of a laser-colored 5 kg silver coin of diameter 21 cm and thickness 2.5 cm [the butterfly coin of (d) is also shown for comparison]. (f) Close up of (e) showing crevices $\sim 5\ \text{mm}$ deep of black and white-colored eyes. (g) Alternate coloring of another 5 kg coin over topographic relief $\sim 1\ \text{cm}$ in height. (h) Close up of (g) near the nose and brow, the highest points on the coin. (i) Angle-independent colors produced on the surface of a gold coin. Reproduced with permission from Guay *et al.*, *Nat. Commun.* **8**, 16095 (2017). Copyright 2017 Springer Nature Publishing AG.

and visual colors can be modified. The absorption peak is sensitive to the nanoparticle size, the dielectric constant of the metal material, and the dielectric properties of the ambiances. Therefore, the visual color can be tuned by controlling these factors. The laser-induced nanostructures are often randomly distributed on the sample surface and consist of one or more of the following structures: nanocavities, nanoholes, nanoprotusions, and nanoparticles. Different mechanisms are proposed to explain the formation of the laser-induced nanostructures, such as hydrodynamic process of laser-induced melt,⁷⁴ cavitation nanopallation,⁷⁵ and nanoparticle redeposition process.⁷⁶

Angle-independent blue color on the Ti surface produced by a femtosecond laser has been demonstrated.⁶⁶ The morphological analyses show that irregular and dense nanostructures are generated on the sample surfaces. Wavelength dependent reflectance of the blue surface reveals that the surface absorptions of green and red light are higher than that those of blue light. The author suggested that this property results from the irregular surface nanostructures, which excite a higher plasmonic absorption at green and red wavelengths than that at blue wavelength. Fan *et al.* reported the simultaneous generation of nanostructures and redeposited nanoparticles on copper surfaces through direct picosecond laser processing in air.²⁶ The produced surface colors do not vary with viewing angle but vary with particle size and mean particle distance. The unique optical properties under a broad range of viewing angles are attributed to the spherical shape and the randomly distribution nanoparticles on the irregularly nanostructured copper surfaces. Guay *et al.* presented a bottom-up approach for noniridescent coloring of metal surfaces and demonstrated the process by colorizing silver coins and Au, Cu, and Al surfaces,⁸ as shown in Fig. 14. This technique is able to produce a complete Hue palette covering the entire spectral region, as plotted in Fig. 15. The remarkable feature is that blue, red, and yellow colors have relative high chroma, while the green and cyan colors have the lowest chroma. Numerical simulation shows that the colors originate from the random distributions of small and medium nanoparticles embedded inside the surface, and the plasmonic resonances play a key role in the color formation. The above-mentioned

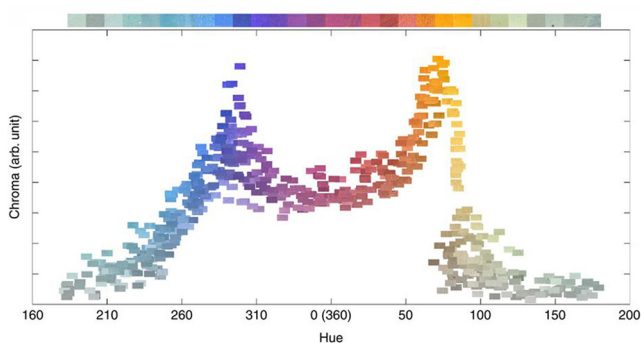


FIG. 15. Graph of chroma vs hue obtained from a collection of color palettes.⁸ The colors are produced by using different processing parameters and the same laser fluence. The horizontal color bar at the top is constructed from a collection of photographs of the 30 highest chroma colors. Reproduced with permission from Guay *et al.*, *Nat. Commun.* **8**, 16095 (2017). Copyright 2017 Springer Nature Publishing AG.

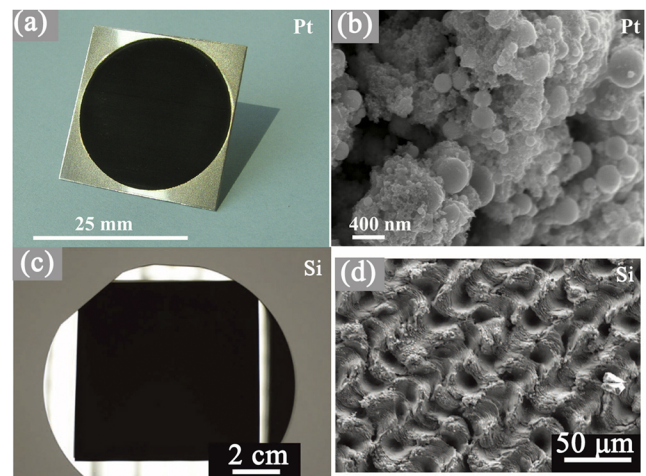


FIG. 16. (a) Photograph of a black Pt sample.⁷⁹ (b) SEM image shows the detailed nanostructures on the Pt surface. [(a) and (b)] Reproduced with permission from A. Vorobyev and C. Guo, *J. Appl. Phys.* **117**(3), 033103 (2015). Copyright 2015 AIP Publishing LLC. (c) Photograph of a textured black Si surface.⁸² (d) SEM image shows the detailed microstructures on the Si surface. [(c) and (d)] Reproduced with permission from Yang *et al.*, *Light: Sci. Appl.* **3**(7), e185 (2014). Copyright 2014 Springer Nature Publishing AG.

research studies of the laser coloration are all carried out in air. The formation of nanostructures has also been demonstrated on Al and Ag surfaces in water and ethanol.^{74,77,78} The nanostructures modify the absorption spectra of the laser treated surfaces and extend the wings of the absorption peak to the visible, leading to a distinct yellow coloration.

Through the controlling of surface optical property, laser direct processing allows us to create not only colorful surfaces but also black surface on metals or semiconductors. The black color can enhance the surface absorption over the whole visible spectrum range via laser structuring of micro/nanoscales and has been demonstrated on a variety of metals, such as Pt,⁷⁹ stainless steel,⁸⁰ Al,^{6,80,81} Cu,^{80,81} and semiconductor material Si.^{82–85} Figure 16 shows the examples of blackened Pt and Si samples, where micro/nanostructures produced on the sample surfaces are considered as the origins for the large absorption. For metals, the physics mechanism underlying the laser blackening is suggested to be broadband surface plasmon absorption induced by various sizes and shapes of subwavelength structures and particles.^{73,86} While for Si material, the large absorption is attributed to surface structures with high aspect ratios, which lead to multiple reflections of light inside the structured surface.^{82,87}

VI. DISCUSSION AND COMPARISON

There are several major concerns with regard to the practical applications of the laser color marking techniques: color stability, operation cost, productivity, and resolution. In this section, a comparison of the three laser coloration techniques is made, in terms of their important performances on these major concerns. The results are shown in Table II.

TABLE II. A comparison of the three laser coloration techniques presented in this article, in terms of their performances on color stability, operation cost, productivity, and resolution.

Technique	Surface oxidation	LIPSS	Nanostructures/particles
Stability	High	Moderate	Low
Operation cost	Low	High	High
Productivity	High (0.5–60 mm ² /s)	Low (0.005–0.8 mm ² /s)	Moderate (0.1–36 mm ² /s)
Resolution (focused beam spot) (μm)	13–350	5–300	14–50

Color stability describes the ability of a color surface to maintain its color properties over time. It is an important index for evaluating the performance of surface coloration techniques. For color coloration by laser-induced oxidation, the stability has been studied by evaluating the ageing and corrosion properties of surface colors.^{10,88} Although laser treatment and harsh environment can affect the surface properties, the corrosion resistance and color durability are stable enough at a normal use condition if the parameters are properly set. It is evident that the color stability obtained from LIPSSs and nanoparticles/structures is not high enough for long-term uses⁸⁹ because the subwavelength structures and nanoparticles/structures are easily oxidized in air. The smaller the structure is, the easier the oxidation is. Therefore, the color stability obtained from the LIPSSs method is higher than that obtained from the laser-induced nanoparticle/structure method. However, the stability can be improved by coating a protection film via atomic layer deposition or evaporation.^{8,89}

As discussed above, the laser coloration technology does not use consumables except electric power. A typical laser coloration machine consumes about hundreds of watts power. It is a green manufacturing technology with low energy consuming. Actually, the biggest expense of laser coloration is the equipment, which is much different depending on the methods of laser coloration. The laser-induced oxidation method uses low-cost CW or nanosecond lasers, while the other two methods require picosecond or femtosecond lasers, which are much more expensive than nanosecond lasers. With the development of laser technology, in general, the laser price has been declining a lot in recent years.

The productivity of laser coloration technology is highly dependent on the substrate properties and processing parameters, such as power, pulse width, pulse repetition rate, scanning speed, and line spacing. Generally speaking, the productivity is directly proportional to the scanning speed and inversely proportional to the line spacing, and larger laser power is conducive to high scanning speed. However, the increasing of scanning speed is limited by the pulse repetition rate and the desired color, which determines the processing parameters for a given substrate. In addition, the coloration methods by LIPSSs and laser-induced nanostructures/particles are usually less efficient. This is because the lasers (pico/femtosecond lasers) used in these two methods are often operating on lower repetition rates. According to the scanning speed and line spacing provided in some research, we calculate some typical productivities of the three laser coloration methods presented in this article, as shown in Table II.

Comparing with the traditional surface coloration methods, laser coloration is better at selective coloring and multiple colors at a time due to its high resolution and simple process. In theory, the

laser coloration technology can produce a small color area down to a focused laser spot, and so the resolution is related to focus length and beam quality. There is little difference in resolution between the three laser coloration methods. Typically, resolution of the laser coloration varies from 5 to 300 μm . Higher resolution is also available by tightly focusing the laser beam, but at the cost of productivity.

VII. SUMMARY

Laser processing has shown itself to be an impressive technique for surface coloration, offering clear benefits of high resolution, single-step process, and flexibility in processing parameters. Laser color marking is achieved by producing surface structures or oxidation films under the laser irradiation, which lead to the modification of optical properties in the visible range. According to the physics mechanisms, there are three main approaches to realize the surface colorizing: (1) laser induced oxidation and the thin film effect, or intrinsic colors of the oxides, (2) LIPSSs and their diffraction, giving rise to iridescent colors, and (3) laser induced nanostructures and nanoparticles, which lead to high absorption at some wavelengths due to the SPR effect. Recent advancements of laser color marking based on each approach are presented. The physics mechanisms underlying the laser color marking techniques are discussed in detail. The resulting surface colors are related to a range of conditions and parameters, including laser processing parameters, ambient condition (temperature), and material properties. The effects of these conditions and parameters on the final colors are also discussed. As presented in this paper, most studies of laser color marking focused on metals and alloys. It is demonstrated that the laser color marking technique is capable of producing complete Hue palettes on metal surfaces through the precise control of laser processing parameters. The laser color marking can find a number of applications in fashion jewelry, souvenirs, product identification and tracking (QR code or barcode), personalized gifts, and anticounterfeiting. The produced colors are sensitive to process parameters, environmental conditions, and material properties. It is essential to improve the repeatability and stability of the process to reduce the influences of the changes of environment and materials. In addition, further research and application tests are needed to determine the optical, wear, corrosion, and scratch properties of the colorized surfaces.

ACKNOWLEDGMENTS

This work was supported by grant from the RIE2020 Advanced Manufacturing and Engineering Individual Research (Grant No.

A1883c0010) and the Fund of National Engineering Research Center for Optoelectronic Crystalline Materials.

REFERENCES

- ¹J. Qi, K. Wang, and Y. Zhu, *J. Mater. Process. Technol.* **139**(1-3), 273–276 (2003).
- ²A. Carey, W. Steen, and D. Watkins, paper presented at the International Congress on Applications of Lasers & Electro-Optics, Orlando, FL, USA, 1998.
- ³S. O'Hana, A. J. Pinkerton, K. Shoba, A. Gale, and L. Li, *Surf. Eng.* **24**(2), 147–153 (2008).
- ⁴A. P. Del Pino, J. Fernández-Pradas, P. Serra, and J. Morenza, *Surf. Coat. Technol.* **187**(1), 106–112 (2004).
- ⁵H. Zheng, G. Lim, X. Wang, J. Tan, and J. Hilfiker, *J. Laser Appl.* **14**(4), 215–220 (2002).
- ⁶A. Y. Vorobyev and C. Guo, *Appl. Phys. Lett.* **92**(4), 041914 (2008).
- ⁷B. Dusser, Z. Sagan, H. Soder, N. Faure, J.-P. Colombier, M. Jourlin, and E. Audouard, *Opt. Express* **18**(3), 2913–2924 (2010).
- ⁸J.-M. Guay, A. C. Lesina, G. Côté, M. Charron, D. Poitras, L. Ramunno, P. Berini, and A. Weck, *Nat. Commun.* **8**, 16095 (2017).
- ⁹Y. Lu, X. Shi, Z. Huang, T. Li, M. Zhang, J. Czajkowski, T. Fabritius, M. Huttula, and W. Cao, *Sci. Rep.* **7**(1), 7092 (2017).
- ¹⁰A. J. Antończak, D. Kocoń, M. Nowak, P. Kozioł, and K. M. Abramski, *Appl. Surf. Sci.* **264**, 229–236 (2013).
- ¹¹Z. Li, H. Zheng, K. Teh, Y. Liu, G. Lim, H. Seng, and N. Yakovlev, *Appl. Surf. Sci.* **256**(5), 1582–1588 (2009).
- ¹²V. Veiko, G. Odintsova, E. Ageev, Y. Karlagina, A. Loginov, A. Skuratova, and E. Gorbunova, *Opt. Express* **22**(20), 24342–24347 (2014).
- ¹³E. Amara, F. Haïd, and A. Noukaz, *Appl. Surf. Sci.* **351**, 1–12 (2015).
- ¹⁴A. P. Del Pino, P. Serra, and J. Morenza, *Thin Solid Films* **415**(1-2), 201–205 (2002).
- ¹⁵D. Adams, R. Murphy, D. Saiz, D. Hirschfeld, M. Rodriguez, P. Kotula, and B. Jared, *Surf. Coat. Technol.* **248**, 38–45 (2014).
- ¹⁶T. Jwad, S. Deng, H. Butt, and S. Dimov, *Appl. Surf. Sci.* **387**, 617–624 (2016).
- ¹⁷Y. Lu and H. Qiu, *J. Appl. Phys.* **88**(2), 1082–1087 (2000).
- ¹⁸J. Yao, C. Zhang, H. Liu, Q. Dai, L. Wu, S. Lan, A. V. Gopal, V. A. Trofimov, and T. M. Lysak, *Appl. Surf. Sci.* **258**(19), 7625–7632 (2012).
- ¹⁹G. Li, J. Li, Y. Hu, C. Zhang, X. Li, J. Chu, and W. Huang, *Appl. Phys. A* **118**(4), 1189–1196 (2015).
- ²⁰J. Long, P. Fan, M. Zhong, H. Zhang, Y. Xie, and C. Lin, *Appl. Surf. Sci.* **311**, 461–467 (2014).
- ²¹A. Vorobyev and C. Guo, *J. Appl. Phys.* **103**(4), 043513 (2008).
- ²²G. Li, J. Li, L. Yang, X. Li, Y. Hu, J. Chu, and W. Huang, *Appl. Surf. Sci.* **276**, 203–209 (2013).
- ²³A. A. Ionin, S. I. Kudryashov, S. V. Makarov, L. V. Seleznev, D. V. Sinityn, E. V. Golosov, A. G. Ol'ga, Y. R. Kolobov, and A. E. Ligachev, *Appl. Phys. A* **107**(2), 301–305 (2012).
- ²⁴A. Vorobyev and C. Guo, *Opt. Express* **19**(105), A1031–A1036 (2011).
- ²⁵C.-Y. Zhang, J.-W. Yao, H.-Y. Liu, Q.-F. Dai, L.-J. Wu, S. Lan, V. A. Trofimov, and T. M. Lysak, *Opt. Lett.* **37**(6), 1106–1108 (2012).
- ²⁶P. Fan, M. Zhong, L. Li, P. Schmitz, C. Lin, J. Long, and H. Zhang, *J. Appl. Phys.* **115**(12), 124302 (2014).
- ²⁷I. Boyd, J. Wilson, and J. West, *Thin Solid Films* **83**(4), L173–L176 (1981).
- ²⁸M. Wautelet and L. Baufay, *Thin Solid Films* **100**(1), L9–L12 (1983).
- ²⁹M. Wautelet, *Mater. Lett.* **2**(1), 20–22 (1983).
- ³⁰L. Baufay, F. Houle, and R. Wilson, *J. Appl. Phys.* **61**(9), 4640–4651 (1987).
- ³¹C. Langlade, A. Vannes, J. Krafft, and J. Martin, *Surf. Coat. Technol.* **100**, 383–387 (1998).
- ³²K. Łęcka, A. Antończak, B. Szubzda, M. Wójcik, B. Stępak, P. Szymczyk, M. Trzciński, M. Ozimek, and K. Abramski, *J. Laser Appl.* **28**(3), 032009 (2016).
- ³³D. P. Adams, V. Hodges, D. Hirschfeld, M. A. Rodriguez, J. McDonald, and P. G. Kotula, *Surf. Coat. Technol.* **222**, 1–8 (2013).
- ³⁴A. Lehmuskero, V. Kontturi, J. Hiltunen, and M. Kuitinen, *Appl. Phys. B* **98**(2-3), 497–500 (2010).
- ³⁵L. Ming, A. Hoult, and A. Tse, paper presented at the Pacific International Conference on Applications of Lasers and Optics, Beijing, China, 2008.
- ³⁶P. Laakso, S. Ruotsalainen, H. Panssar, and R. Penttilä, paper presented at the 12th Conference on Laser Processing of Materials in the Nordic Countries (NOLAMP), Copenhagen, Denmark, 2009.
- ³⁷V. Veiko, G. Odintsova, E. Gorbunova, E. Ageev, A. Shimko, Y. Karlagina, and Y. Andreeva, *Mater. Des.* **89**, 684–688 (2016).
- ³⁸A. P. Del Pino, P. Serra, and J. Morenza, *Appl. Surf. Sci.* **197**, 887–890 (2002).
- ³⁹H. Ghorbani, M. H. Sohi, M. J. Torkamany, and B. Mehrjou, *J. Mater. Eng. Perform.* **24**(9), 3634–3642 (2015).
- ⁴⁰A. J. Antończak, Ł. Skowroński, M. Trzcinski, V. V. Kinzhybalov, Ł. K. Łazarek, and K. M. Abramski, *Appl. Surf. Sci.* **325**, 217–226 (2015).
- ⁴¹E. György, A. P. Del Pino, P. Serra, and J. Morenza, *Appl. Phys. A* **78**(5), 765–770 (2004).
- ⁴²L. Nánai, R. Vajtai, and T. F. George, *Thin Solid Films* **298**(1-2), 160–164 (1997).
- ⁴³L. Lavis, J. Jouvard, L. Imhoff, O. Heintz, J. Korntheuer, C. Langlade, S. Bourgeois, and M. M. de Lucas, *Appl. Surf. Sci.* **253**(19), 8226–8230 (2007).
- ⁴⁴H. Y. Zheng and G. C. Lim, U.S. patent US6613161B2 (2 September 2003).
- ⁴⁵F. Luo, W. Ong, Y. Guan, F. Li, S. Sun, G. Lim, and M. Hong, *Appl. Surf. Sci.* **328**, 405–409 (2015).
- ⁴⁶R. Zhou, T. Huang, Y. Lu, and M. Hong, *Appl. Sci.* **8**(10), 1716 (2018).
- ⁴⁷A. R. Parker, *J. Opt. A: Pure Appl. Opt.* **2**(6), R15 (2000).
- ⁴⁸M. Birnbaum, *J. Appl. Phys.* **36**(11), 3688–3689 (1965).
- ⁴⁹A. Borowiec and H. Haugen, *Appl. Phys. Lett.* **82**(25), 4462–4464 (2003).
- ⁵⁰J. Bonse, J. Krüger, S. Höhm, and A. Rosenfeld, *J. Laser Appl.* **24**(4), 042006 (2012).
- ⁵¹K. Okamoto, M. Hashida, Y. Miyasaka, Y. Ikuta, S. Tokita, and S. Sakabe, *Phys. Rev. B* **82**(16), 165417 (2010).
- ⁵²C. Hnatovsky, R. Taylor, P. Rajeev, E. Simova, V. Bhardwaj, D. Rayner, and P. Corkum, *Appl. Phys. Lett.* **87**(1), 014104 (2005).
- ⁵³H.-D. Yang, X.-H. Li, G.-Q. Li, C. Wen, R. Qiu, W.-H. Huang, and J.-B. Wang, *Appl. Phys. A* **104**(2), 749–753 (2011).
- ⁵⁴J. Sipe, J. F. Young, J. Preston, and H. Van Driel, *Phys. Rev. B* **27**(2), 1141 (1983).
- ⁵⁵K. Ahmed, C. Grambow, and A.-M. Kietzig, *Micromachines* **5**(4), 1219–1253 (2014).
- ⁵⁶J. F. Young, J. Preston, H. Van Driel, and J. Sipe, *Phys. Rev. B* **27**(2), 1155 (1983).
- ⁵⁷R. Buividas, M. Mikutis, and S. Juodkakis, *Prog. Quantum Electron.* **38**(3), 119–156 (2014).
- ⁵⁸S. Sakabe, M. Hashida, S. Tokita, S. Namba, and K. Okamoto, *Phys. Rev. B* **79**(3), 033409 (2009).
- ⁵⁹A. M. Bonch-Bruевич, M. N. Libenson, V. S. Makin, and V. V. Trubaev, *Opt. Eng.* **31**(4), 718–731 (1992).
- ⁶⁰A. V. Zayats and I. I. Smolyaninov, *J. Opt. A: Pure Appl. Opt.* **5**(4), S16 (2003).
- ⁶¹A. Vorobyev, V. Makin, and C. Guo, *J. Appl. Phys.* **101**(3), 034903 (2007).
- ⁶²M. Huang, F. Zhao, Y. Cheng, N. Xu, and Z. Xu, *Opt. Express* **18**(104), A600–A619 (2010).
- ⁶³L. Qi, K. Nishii, and Y. Namba, *Opt. Lett.* **34**(12), 1846–1848 (2009).
- ⁶⁴V. Makin, R. Makin, A. Y. Vorobyev, and C. Guo, *Tech. Phys. Lett.* **34**(5), 387–390 (2008).
- ⁶⁵O. Varlamova, J. Reif, S. Varlamov, and M. Bestehorn, *J. Nanosci. Nanotechnol.* **11**(10), 9274–9281 (2011).
- ⁶⁶A. Y. Vorobyev and C. Guo, *Laser Photonics Rev.* **7**(3), 385–407 (2013).
- ⁶⁷A. Vorobyev and C. Guo, *J. Appl. Phys.* **104**(6), 063523 (2008).
- ⁶⁸T. Y. Hwang and C. Guo, *J. Appl. Phys.* **108**(7), 073523 (2010).
- ⁶⁹V. P. Korol'kov, A. A. Ionin, S. I. Kudryashov, L. V. Seleznev, D. V. Sinityn, R. Samsonov, A. I. Maslii, A. Z. Medvedev, and B. Gol'denberg, *Quantum Electron.* **41**(4), 387 (2011).
- ⁷⁰M. Shen, J. E. Carey, C. H. Crouch, M. Kandyla, H. A. Stone, and E. Mazur, *Nano Lett.* **8**(7), 2087–2091 (2008).
- ⁷¹K. A. Willets and R. P. Van Duyne, *Annu. Rev. Phys. Chem.* **58**, 267–297 (2007).

- ⁷²J. Tong, F. Suo, J. Ma, L. Tobing, Y. M. L. Qian, and D. H. Zhang, *Opto-Electron. Adv.* **2**(1), 180026 (2019).
- ⁷³J. Z. Zhang and C. Noguez, *Plasmonics* **3**(4), 127–150 (2008).
- ⁷⁴E. Stratakis, V. Zorba, M. Barberoglou, C. Fotakis, and G. Shafeev, *Nanotechnology* **20**(10), 105303 (2009).
- ⁷⁵V. V. Zhakhovskii, N. A. Inogamov, and K. Nishihara, *JETP Lett.* **87**(8), 423–427 (2008).
- ⁷⁶A. Pereira, A. Cros, P. Delaporte, S. Georgiou, A. Manousaki, W. Marine, and M. Sentis, *Appl. Phys. A* **79**(4-6), 1433–1437 (2004).
- ⁷⁷E. Stratakis, V. Zorba, M. Barberoglou, C. Fotakis, and G. Shafeev, *Appl. Surf. Sci.* **255**(10), 5346–5350 (2009).
- ⁷⁸E. V. Zavedeev, A. Petrovskaya, A. V. Simakin, and G. A. Shafeev, *Quantum Electron.* **36**(10), 978 (2006).
- ⁷⁹A. Vorobyev and C. Guo, *J. Appl. Phys.* **117**(3), 033103 (2015).
- ⁸⁰V. V. Iyengar, B. K. Nayak, and M. C. Gupta, *Appl. Opt.* **49**(31), 5983–5988 (2010).
- ⁸¹H. Huang, L.-M. Yang, S. Bai, and J. Liu, *Appl. Opt.* **54**(2), 324–333 (2015).
- ⁸²J. Yang, F. Luo, T. S. Kao, X. Li, G. W. Ho, J. Teng, X. Luo, and M. Hong, *Light: Sci. Appl.* **3**(7), e185 (2014).
- ⁸³C. Wu, C. Crouch, L. Zhao, J. Carey, R. Younkin, J. Levinson, E. Mazur, R. Farrell, P. Gothoskar, and A. Karger, *Appl. Phys. Lett.* **78**(13), 1850–1852 (2001).
- ⁸⁴M. A. Sheehy, L. Winston, J. E. Carey, C. M. Friend, and E. Mazur, *Chem. Mater.* **17**(14), 3582–3586 (2005).
- ⁸⁵R. Zhou, S. Lin, Y. Ding, H. Yang, K. O. Y. Keng, and M. Hong, *Opto-Electron. Adv.* **1**(08), 180014 (2018).
- ⁸⁶K. L. Kelly, E. Coronado, L. L. Zhao, and G. C. Schatz, *J. Phys. Chem. B* **107**(3), 668–677 (2003).
- ⁸⁷C. H. Crouch, J. Carey, M. Shen, E. Mazur, and F. Genin, *Appl. Phys. A* **79**(7), 1635–1641 (2004).
- ⁸⁸M. Švantner, M. Kučera, E. Smazalová, Š. Houdková, and R. Čerstvý, *Appl. Opt.* **55**(34), D35–D45 (2016).
- ⁸⁹J.-M. Guay, G. Killaire, P. G. Gordon, S. T. Barry, P. Berini, and A. Weck, *Langmuir* **34**(17), 4998–5010 (2018).